Hindawi
Journal of Nanomaterials
Volume 2021, Article ID 9975600, 9 pages
https://doi.org/10.1155/2021/9975600

Research Article

Optical and Photocatalytic Properties of Cu_xS/ZnO Composite Thin Films Deposited by Robotic Spray Pyrolysis Deposition

Adrien P. Yepseu,[1] Luminita Isac,[2] Linda D. Nyamen,[1] Franck Cleymand,[3] Anca Duta,[2] and Peter T. Ndifon[1]

[1]*Department of Inorganic Chemistry, University of Yaounde I, P.O. Box 812, Yaoundé, Cameroon*
[2]*Transilvania University of Brasov, R&D Center, Renewable Energy Systems and Recycling, Eroilor 29, 500036 Brasov, Romania*
[3]*Institut Jean Lamour UMR CNRS 7198, Université de Lorraine, Nancy, France*

Correspondence should be addressed to Peter T. Ndifon; pndifon@yahoo.com

Received 24 March 2021; Revised 24 May 2021; Accepted 14 June 2021; Published 16 July 2021

Academic Editor: Shijun Liao

This article reports on VIS-active composite thin films based on zinc oxide (ZnO) and copper sulfide (Cu_xS) deposited using robotic spray pyrolysis deposition (SPD) for the study of the optical and photocatalytic properties. The first step involves the SPD deposition of a Cu_xS layer onto the glass substrate at 300°C. The second step consists of the deposition of a ZnO layer onto the Cu_xS layer to form glass/Cu_xS-ZnO composites that were further annealed at 400°C. The development of the composite thin films was confirmed by XRD and EDX analyses. The band gap energy (E_g) of the bare ZnO thin films decreased from 3.15 eV to an activation energy value of 2.8 eV after the deposition of the ZnO thin layer onto the Cu_xS layer and from 2.8 to 2.08 eV after annealing the Cu_xS-ZnO composite at 400°C. The UV-VIS irradiation (5.5% of UV, $G = 55\ W/m^2$) of a 10 ppm methylene blue solution was used to investigate the photocatalytic properties of the Cu_xS-ZnO composites. The annealed Cu_xS-ZnO thin films at 400°C demonstrates better photocatalytic activity compared to Cu_xS-ZnO composites deposited at 300°C. The enhanced photocatalytic efficiency of the annealed Cu_xS-ZnO thin films may be the result of the diode structure and the increased crystallinity that prevent the electron-hole recombination.

1. Introduction

Nowadays, synthetic dyes are widely used in the textile, paper, food, or cosmetic industries. During industrial processes, some of these dyes are released into the wastewater, and their total or partial further release into rivers and lakes produces serious environmental problems [1, 2]. It is therefore necessary to develop a technology that can remove contaminants, as these dyes, that are at low concentration but higher than the discharge limit [3]. In this context, solar photocatalysis is an appropriate option to degrade recalcitrant pollutants in water [4, 5]. During the recent years, a significant effort was directed for using the clean, safe, and abundant solar energy through the development of visible light driven photocatalysts that can support implementing the processes at larger scale.

Semiconductor-based photocatalysts raised considerable attention due to their promising avenue for solving environmental and energy problems, by using the abundant solar radiation. Different metal oxides were reported to exhibit photocatalytic activity, such as TiO_2, ZnO, WO_3, and SnO_2 [6–9]. Among these, the zinc oxide (ZnO) thin film was widely applied in the degradation of organic pollutants from water or air due to its nontoxicity, low cost, photochemical stability, and photocatalytic performance [10, 11]. However, the use of ZnO is limited due to the high recombination rate of the charge carriers and its wide band gap (~3.2 eV) that allows its activation only under UV radiation. In order to overcome these limitations, one of the strategies is to reduce the required activation energy by coupling the n-type ZnO semiconductor with a lower band gap p-type semiconductor with suitably aligned energy bands to form diode-type

heterostructures able to extend the photocatalytic response towards VIS [10, 11].

Transition metal sulfides are usually coloured; thus, they absorb radiation in the VIS spectral range and are therefore promising candidates for solar cells and photocatalytic applications [12, 13]. Among the transition metal sulfides, CdS and PbS have been combined with ZnO to develop suitable heterojunctions, and these heterostructures are also applicable in VIS-activated photocatalysis [14, 15]. However, Cd and Pb are highly toxic elements; thus, an alternative material is required for obtaining more environmental friendly photocatalysts. Environmental friendly copper sulfide (Cu_xS) materials with Cu vacancies are one of the best choices. Copper sulfide (Cu_xS) is recognized as an important, narrow band gap (1.2-2.1 eV) p-type semiconductor suitable for modifying the properties of ZnO when attached to the ZnO surface to develop n-p heterojunctions, and these heterostructures have applications in VIS-activated photocatalysis [13, 16]. A literature review indicates that work was carried out on the synthesis of powder Cu_xS-ZnO nanocomposites for photocatalytic applications. For example, Li et al. [17] reported the synthesis of three-dimensional (3D) Cu_2S@ZnO composites by an easy three-step synthesis process and showed their efficiency in the degradation of methylene blue; Zhu et al. [18] reported the synthesis of CuS-ZnO nanocomposites by a simple mechanical method, without adding surfactants. The photocatalytic efficiency of the nanocomposites reached the highest value when 0.5% CuS was added to ZnO; Hong et al. developed a CuS-ZnO nanowire array using a stainless-steel mesh, and ZnO-CuS heterostructured nanoarrays were widely used in piezophotocatalytic activity for the degradation of methylene blue [19]. Morevoer, Silvie et al. reported the synthesis of ZnO-CuS nanocomposites by the hydrothermal method using two sulfur sources, thiourea and thioglycolic acid, and showed their efficiency in the degradation of the Mordant Black 11 dye [20]. However, the use of powder photocatalysts suspended in water raises two major problems specific particularly for small-sized powder grains: the catalyst separation after the photocatalytic process from the aqueous solution and its recycling for reuse.

To overcome these problems, Cu_xS-ZnO photocatalysts can be used as thin films. The use of films in industrial processes is recommended as avoiding the technological problems raised by powder leaching, aggregation, and/or separation.

There are only a few publications reporting on Cu_xS-ZnO thin films such as Zhang et al. that have deposited a CuS-ZnO composite film on a quartz substrate using a spin coating method, and the tribological effect of the CuS addition to the ZnO thin fillm was investigated [21]. The thin films should be obtained using a low-cost, low-energy deposition method that can be easily scaled up. To meet these requirements, Cu_xS-ZnO thin films were deposited by robotic spray pyrolysis (R-SPD) that was identified as an inexpensive and versatile technique for the thin films deposition [22].

This paper reports on the deposition of a ZnO thin film on a Cu_xS thin film using the robotic spray pyrolysis route. After deposition, the Cu_xS-ZnO composite thin films were annealed at 400°C to improve the crystallinity and the interface interactions between the two layers. The structural, morphological, and optical properties of Cu_xS-ZnO composites before and after annealing were further investigated to outline their influence on the photocatalytic response.

2. Experimental Section

2.1. Chemicals. $CuCl_2{\cdot}2H_2O$ (99%, Scharlau Chemie SA), thiourea H_2NCSNH_2 (99%, Scharlau Chemie SA), $ZnCl_2$ (99.99%, Scharlau Chemie SA), absolute ethanol (C_2H_5OH, 99.2%, SC PAM Corporation SRL, Bucharest), and glycerol ($C_3H_8O_3$, 99.5%, Scharlau Chemie SA) were obtained from commercial sources and used without any further purification.

2.2. Instrumentation. The crystallinity of the thin films was investigated using a Bruker D8 Discover X-ray Diffractometer ($CuK_\alpha = 1.5406$ Å, locked-couple technique, step size 0.02, scan speed 3 s/step, 2θ range from 20 to 70°). Scanning electron microscopy (SEM) was employed to observe the thin film surface using a Hitachi SEM S-3400 N type 121 II device coupled with a ThermoScienctificUltra Dry energy dispersive X-ray spectrometer (EDX). The topography of the composites was investigated via Atomic Force Microscopy (AFM, NT-MDT model BL222RNTE). The band gap and activation energy values of the thin films were estimated using a UV-VIS-NIR spectrophotometer (Perkin Elmer Lambda 950).

2.3. Thin Film Deposition

2.3.1. Cu_xS Thin Films. Cu_xS films were deposited by robotic spay pyrolysis using 50 mL solution containing the precursors mix ($CuCl_2.2H_2O$ and thiourea, H_2NCSNH_2) dissolved in a 7 : 2 : 1 volume ratio of deionized water : absolute ethanol : glycerol. The Cu : S molar ratio in the precursor solution was 1 : 3 at a 0.3 mol/L Cu^{2+} concentration. This solution was sprayed on a glass substrate (1.5 cm × 1.5 cm) heated at 300°C, using 25 spraying sequences, with 30-second break between two consecutive spraying pulses and air as carrier gas. The glass substrates were previously cleaned with water and detergent at neutral pH followed by ultrasonication in ethanol and then dried using an air compressor. These deposition parameters were the result of previously optimized data [16, 23].

2.3.2. Cu_xS-ZnO Composite Films. $ZnCl_2$ was dissolved in a 7 : 3 volume ratio of water : ethanol to obtain 50 mL of 0.1 M solution. This precursor solution was sprayed on the glass/-Cu_xS substrates heated at 300°C, using 10 spraying sequences, with 45-second break between two consecutive spraying pulses [23] using air as carrier gas. Annealing at 400°C for one hour was further used to increase the crystallinity of the two-layered structure.

2.4. Photocatalytic Experiments. The photodegradation experiments were run in a quartz beaker using two UV radiation sources (UV-A, typically 340-400 nm, $\lambda_{UV,max} = 365$ nm, Philips) and five VIS light sources (TL-D Super 80 18W/865, typically 400-700 nm, $\lambda_{VIS,max} = 565$ nm, Philips), with a total average irradiance value of 55 W/m^2. The UV

contribution to the total irradiance represents approximately 5.5%, which resembles the profile of a simulated solar radiation at much lower irradiance value. A 0.0125 mM (10 ppm) methylene blue solution (MB, 99.8%, Merck) was prepared, as recommended by the standard ISO 10678:2010, [24], using ultrapure water (Direct-Q3 Water Purification System). In each experiment, a composite thin film was immersed in 20 mL of MB solution corresponding to a 2 cm thick liquid layer above the sample, allowing thus minimal radiation losses. Prior to irradiation, the samples were kept one hour in dark to reach the adsorption-desorption equilibrium. The photodegradation efficiency (η) was calculated based on the initial absorbance of the dye solution (A_0) and the absorbance after 1, 2, 4, and 6 hours (A_t), recorded at the maximum absorbance wavelength for MB ($\lambda = 663$ nm), using a UV-VIS-NIR spectrophotometer (Perkin Elmer Lambda 950), according to the following equation[24]:

$$\eta = \frac{Ao - At}{Ao} \times 100. \quad (1)$$

3. Results and Discussions

3.1. Structure, Surface Morphology, and Composition. The structural properties of the ZnO thin film and of the Cu_xS-ZnO composite layers obtained by depositing the ZnO thin layers over the Cu_xS layer at 300°C and further annealed at 400°C were studied, and the XRD patterns are inserted in Figure 1.

All diffraction peaks of the ZnO thin films in Figure 1(a) can be assigned to the hexagonal structure (JCPDS-00-065-0726). A strong orientation is observed along the (002) plane that represents the growth perpendicular to the substrate surface and indicate that the ZnO thin films are strongly oriented along the *c*-axis [25, 26]. The (002) plane of the ZnO thin film represents the most thermodynamically favorable growth plane due to its low surface energy and the most dense wurtzite structure [27]. A decrease in the (002) peak intensity was observed after the deposition of ZnO on Cu_xS (Figure 1(b)), indicating that the orientation of the bare ZnO films along the (002) direction was altered when grown on Cu_xS due to a decrease in the atomic diffusion between the Cu_xS and ZnO films. The XRD data for the Cu_xS-ZnO composite deposited at 300°C (Figure 1(b)) and after annealing at 400°C (Figure 1(c)) show the combinations of two sets of patterns: one assigned to ZnO (JCPDS-01-089-1394) and the other (represented by two asterisks) corresponding to the crystalline structures of $Cu_{1.8}S$ (JCPDS-00-04-0881) [16, 28] and of Cu_2S (JCPDS-01-072-1071) [29, 30]. The XRD patterns of the Cu_xS-ZnO composite deposited at 300°C and after the annealing treatment at 400°C also exhibit the characteristic peaks for the hexagonal structure of the ZnO thin films. The diffractograms outline the relative low crystallinity of Cu_xS compared to ZnO as the Cu_xS peaks are of lower amplitude in the XRD patterns of the Cu_xS-ZnO composite structure. This could also be the consequence of the fact that Cu_xS is not directly exposed to the X-rays. A similar trend was observed for the annealed composites (Figure 1(c)). Additional peaks were observed in the diffractograms that can be attributed to CuO (JCPDS-00-048-1548). The presence of CuO in the thin film is the result of spraying using air as carrier gas, thus supporting the formation of CuO; moreover, the annealing treatment increases this phase in the film. The results also show an increase of about 5% in the crystallinity degree after annealing.

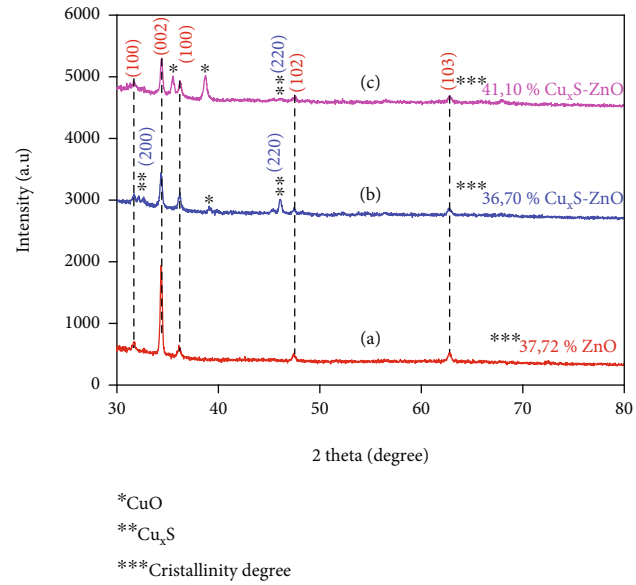

FIGURE 1: XRD patterns of (a) the ZnO thin films, (b) Cu_xS-ZnO composites thin films as deposited, and (c) after annealing at 400°C.

SEM analyses were carried out to investigate the surface morphology of the thin films, and the results are included in Figure 2. The Cu_xS thin films show agglomerated granular particles with cracks (Figure 2(a)) while ZnO thin films are deposited in agglomerated uneven clusters (Figure 2(b)). After deposition of ZnO on glass/Cu_xS, the Cu_xS-ZnO composites show a granular surface (Figure 2(c)) with surface cracks. After annealing at 400°C (Figure 2(d)), the layers have a less compact surface aspect with less surface cracks.

The AFM images of the Cu_xS-ZnO composites deposited at 300°C (Figures 3(a) and 3(b)) and after annealing at 400°C (Figures 3(c) and 3(d)) confirm the results outlined in the SEM images and allow to calculate the average roughness values of 83.47 nm and 145.13 nm, respectively. These values suggest that annealing increases the roughness as a possible result of additional surface reactions (e.g., Cu_xS oxidation). The increase in roughness after annealing can be linked to the growth/aggregation of the smaller grains forming larger and domed grains with micropores. This increase in the roughness values due to spiky and bumpy aggregates may result in more active sites increasing thus the photocatalytic activity [31–34], as a porous surface increases the number of active sites available for the pollutant molecules adsorption as first step in photocatalysis [31, 32].

Energy dispersive X-ray spectroscopy (EDX) was employed to get the elemental surface composition of the composite thin films deposited at 300°C (Table S1) and after annealing at 400°C (Table S2), and the results are included in Table 1. Figures S1 and S1 display their elemental mapping. These results show that the surface

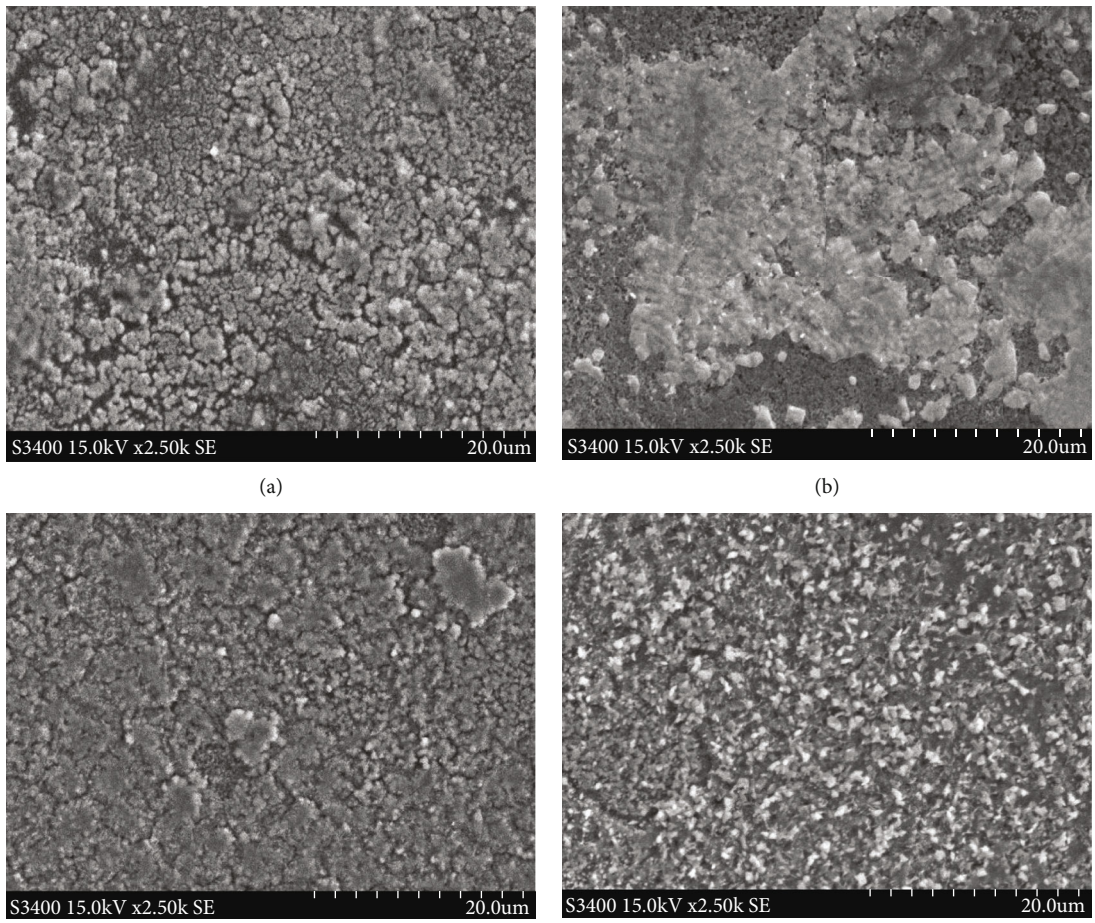

Figure 2: SEM images of (a) Cu_xS thin films, (b) ZnO thin films, (c) Cu_xS-ZnO composite films deposited at 300°C, and (d) Cu_xS-ZnO composite films after annealing at 400°C.

mainly contains Cu, S, Zn, and O in the nanocomposites as deposited at 300°C with a Cu_xS : ZnO ratio of 1 : 2.4 and, after annealing at 400°C, with a ratio of 1 : 2.3. Moreover, the molar ratio of Cu and S was found to be Cu : S = 1.4 : 1 for the Cu_xS-ZnO composites obtained at 300°C and 1.75 : 1 after annealing at 400°C. These results indicate that the molar ratio in the precursor solution (Cu : S = 1 : 3) was changed during the deposition and the annealing treatment and confirm that copper exists as sulfide(s) but also in other compounds as the oxide(s), confirming the XRD results. In addition, other elements (Si, Ca) from the glass substrate were identified, proving that the layers are very thin. The presence of the Cl atoms on the surface of the Cu_xS-ZnO composite thin film as deposited at 300°C is the result of the zinc chloride precursor used for the deposition of ZnO. The excess of oxygen in the Cu_xS-ZnO composites obtained at 300°C may be the result of the absorbed oxygen at the surface during spraying as air was used as carrier gas. It can also be the result of the partial oxidation of Cu_xS to Cu_xO. A large excess of oxygen is also observed in the Cu_xS-ZnO composites after annealing, confirming the increase in the Cu_xO content after annealing in air. These results well corroborate with the XRD data.

3.2. Optical Properties. The transmittance spectra of the bare ZnO and Cu_xS thin films and of the Cu_xS-ZnO composites as deposited at 300°C and after annealing at 400°C are included in Figure 4. The spectrum of the ZnO thin film shows a maximum transmittance of approximately 80% in the VIS region, which is close to the values reported in literature [35], while Cu_xS thin films have a low transmittance value, of maximum 18%. For the Cu_xS-ZnO composite deposited at 300°C, a slight increase in the transmittance, close to 23%, is observed as result of the interaction between the Cu_xS and ZnO thin films and/or as result of the partial oxidation of the Cu_xS thin film. This value increases to approximately 54% in the Cu_xS-ZnO composite after annealing at 400°C. This increase in transmittance may be due to the increase in the grain size and improved structural homogeneity (that avoiding scattering) and crystallinity along with a modified surface composition, as already explained.

The UV-diffuse reflectance spectra of the bare ZnO and Cu_xS thin films and of the Cu_xS-ZnO composites as deposited at 300°C and after annealing at 400°C are included in Figure 5. The results show that ZnO thin film exhibit the highest reflectance throughout the whole VIS region while the reflectance decreases in the VIS region after deposition

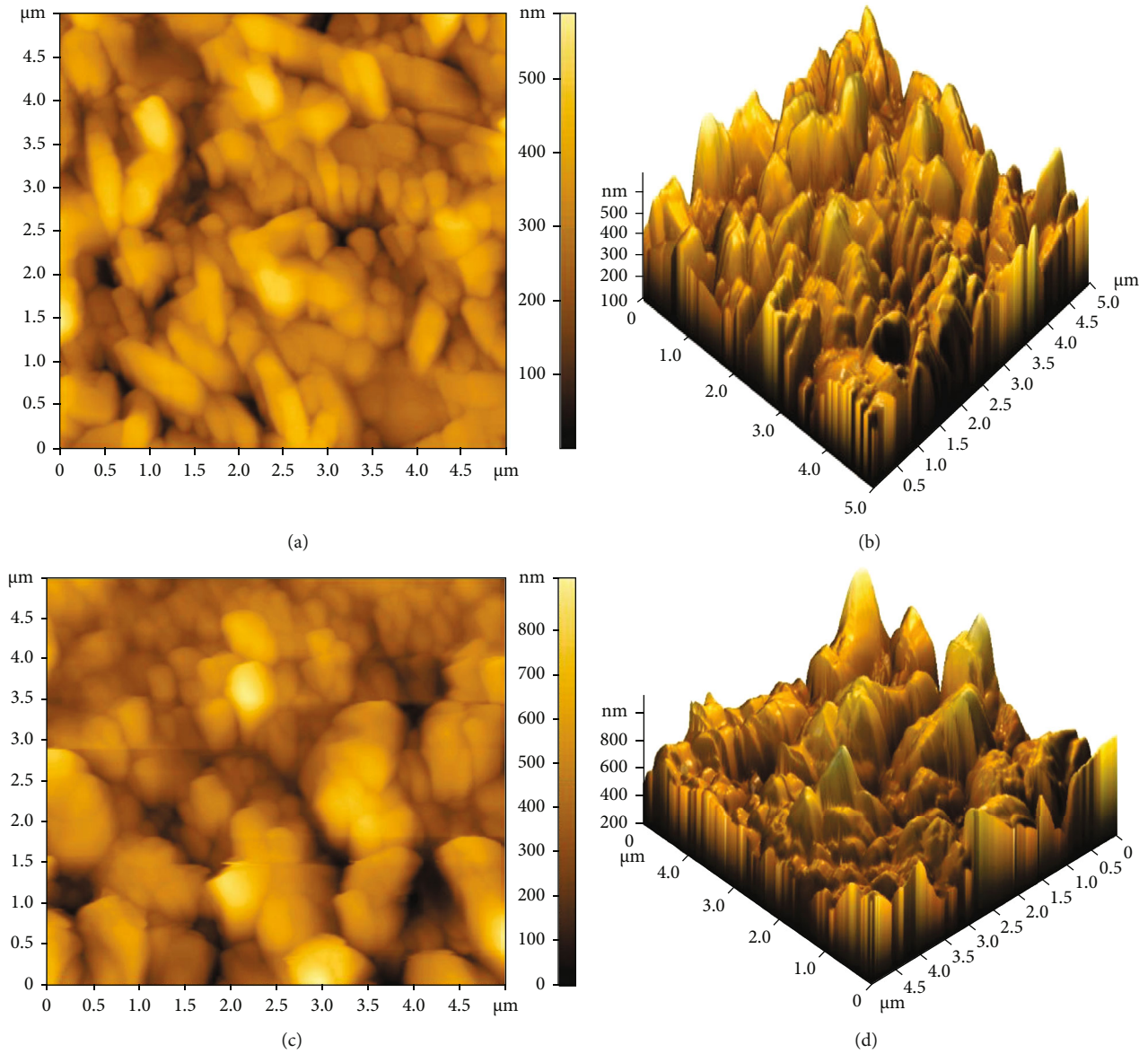

Figure 3: 2D (a, c) and 3D (b, d) AFM images for the Cu_xS-ZnO composites deposited at 300°C (a, b) and after the annealing treatment at 400°C (c, d).

Table 1: EDX results of the Cu_xS-ZnO composites as deposited at 300°C and after treatment at 400°C.

Cu_xS-ZnO as deposited at 300°C		Cu_xS-ZnO after annealing at 400°C	
Elements	Atomic %	Elements	Atomic %
Zn	21.47	Zn	15.28
O	44.28	O	52.30
Cu	15.17	Cu	15.21
S	10.73	S	8.71
Cl	0.89	Cl	—
Si	6.46	Si	7.21
Ca	1.00	Ca	1.28

of ZnO thin film onto Cu_xS and annealing at 400°C, indicating that Cu_xS-ZnO composite thin film obtained after annealing is expected to be a better photocatalyst under VIS irradiation. These results are similar to those reported in literature [36]. Indeed, the Cu_xS layer can support the transport of the photogenerated charges carriers in the ZnO conduction band while suppressing their recombination due to the n-p heterojunction. The heterojunction also supports the alignment of the Fermi levels and therefore facilitates transport of electrons and holes on different paths.

The band gap and activation energy levels for the thin films were estimated using Tauc's plots that correlate the absorption coefficient and the photon energy [37, 38] and are presented in Figure 6. The direct energy band gap calculated for ZnO and for the Cu_xS thin films is 3.15 eV and 2.63 eV, while for the Cu_xS-ZnO composite deposited at 300°C

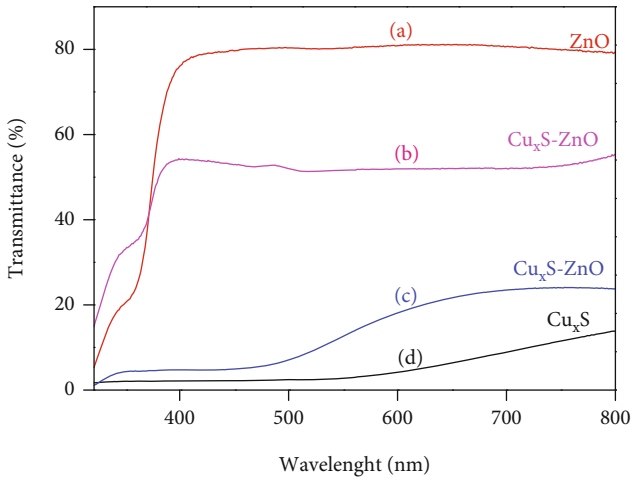

Figure 4: Optical transmittance spectra of (a) ZnO, (b) Cu$_x$S-ZnO after annealing at 400°C, (c) Cu$_x$S-ZnO as deposited at 300°C, and (d) Cu$_x$S.

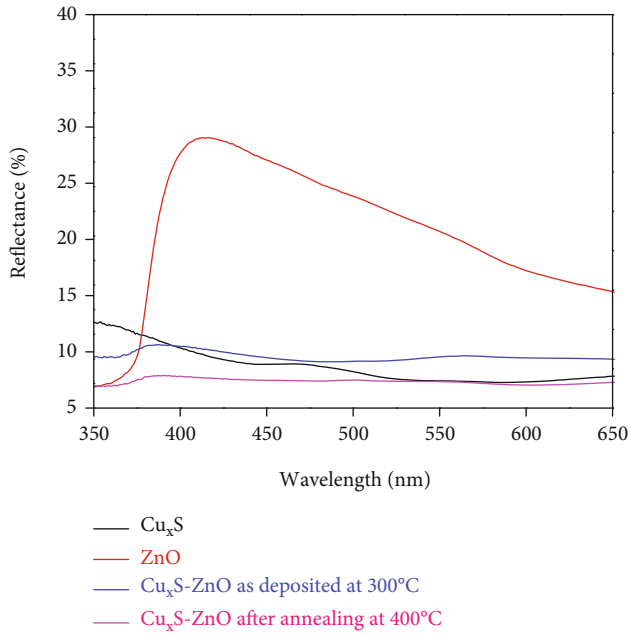

Figure 5: UV-VIS diffuse reflectance spectra of ZnO, Cu$_x$S, and Cu$_x$S-ZnO as deposited at 300°C and after annealing at 400°C.

and for the composite layer after annealing at 400°C, the activation energy was estimated at 2.80 and 2.08 eV, respectively. These values are close to those reported in literature and strongly depend on the composition and crystallinity of the thin films [37, 39]. These results revealed that the energy band gap value of the ZnO thin films was reduced from 3.15 to 2.80 eV after deposition on the Cu$_x$S layer at 300°C that confirms that good interfaces resulted between these two layers. These results also show that the band gap energy of Cu$_x$S-ZnO composite deposited at 300°C decreased from 2.80 to 2.08 eV after annealing, and the values for both composites are proving their VIS activation. This decrease originates from the formation of the diode structure, caused by the alignment of energy bands of ZnO, Cu$_x$S, and Cu$_x$O as illustrated in Figure 7.

3.3. Photocatalytic Activity. The photocatalytic activity of the Cu$_x$S-ZnO composite thin films was evaluated in the degradation of methylene blue under UV-VIS irradiation at low irradiance values at different process durations, and the results are included in Figure 8. The corresponding absorption spectra of the variation with time of Methyl Blue solution under light irradiation are illustrated in Figures S3 and S4. The results show that the photodegradation efficiency is higher when using the Cu$_x$S-ZnO composite deposited at 300°C (Figure 8(a)) compared to that obtained when using the composite after annealing at 400°C (Figure 8(b)) for an initial irradiation duration of 2 hours. After about three hours of irradiation, the removal efficiency on the Cu$_x$S-ZnO composite obtained after annealing at 400°C becomes higher than that of the sample deposited at 300°C as a possible result of a less clogged surface with photocatalytic by-products owing to its more ordered surface aspect (as the results in Figure 2 show) which is one of the key aspects for a higher photocatalytic performance. This is in good agreement with the SEM images. Moreover, the higher photocatalytic efficiency of the composite obtained after annealing at 400°C could also be due to a higher crystallinity degree of the annealed material that leads to better mobility of the photogenerated charge carriers. The improvement of the charge carrier's transport prevents recombination and allows producing more oxidant species such as the hydroxyl radicals. The dye removal efficiency after 1 hour in dark and 6 hours under UV+VIS radiation was 10.35% for the Cu$_x$S-ZnO composites deposited at 300°C and 13.32% for the Cu$_x$S-ZnO composites after annealing at 400°C. The enhanced photocatalytic efficiency of the annealed Cu$_x$S-ZnO thin films can be attributed to the diode structure and the crystallinity that prevents recombination as already outlined. Moreover, the amount of CuO increases after annealing in composite thin films that could also increase the photocatalytic activity; thus, both the CuO content and the increased in crystallinity degree may be responsible for the experimental result.

Considering the low irradiance value used in the experiments (55 W/m^2), significant higher photodegradation efficiencies are to be expected under natural solar radiation (with an average irradiance value of 500-1000 W/m^2).

The results recorded using the Cu$_x$S-ZnO composite deposited at 300°C and after annealing at 400°C represent an improvement over previous results obtained when using TiO$_2$/Cu$_x$S-CuO/SnO$_2$ thin films tested using the same irradiation scenario and using phenol solutions with 4, 10, and 20 ppm concentration. After 6 h of irradiation, the highest recorded efficiency was in that case of 8.75% for the 4 ppm, 6.8% for the 10 ppm, and 6.9% for the 20 ppm pollutant concentration [40].

The use of a Cu$_x$S-ZnO diode structure (p-n semiconductor composite) can lead to an overall decrease in the activation energy of the photocatalytic heterostructure, from the UV wavelength (required by ZnO) to the VIS. The ZnO, Cu$_x$S, and Cu$_x$O semiconductors have different potential

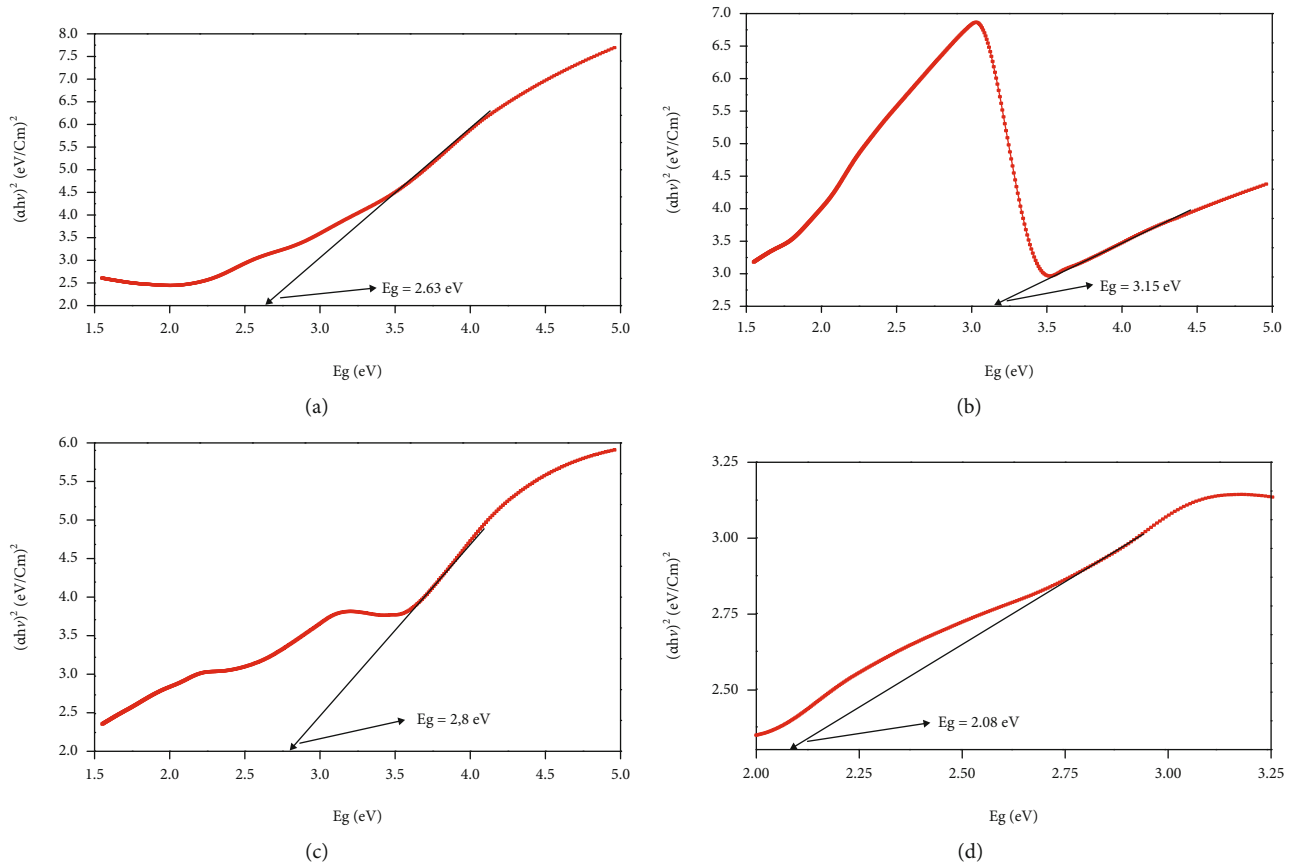

Figure 6: The Tauc plots of (a) Cu_xS, (b) ZnO, and (c) Cu_xS-ZnO nanocomposites as deposited at 300°C and (d) after annealing at 400°C.

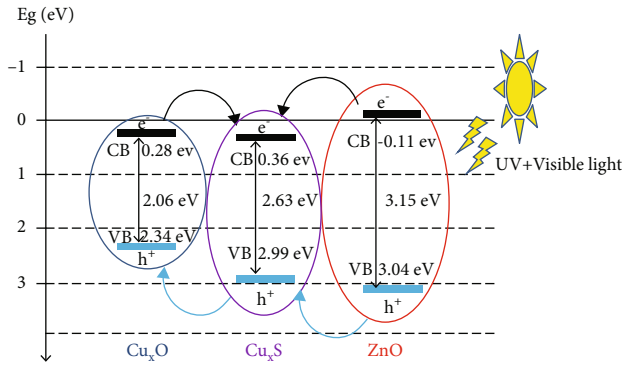

Figure 7: Proposed schematic diagram alignment of energy bands of ZnO, Cu_xS, and Cu_xO in composite thin films.

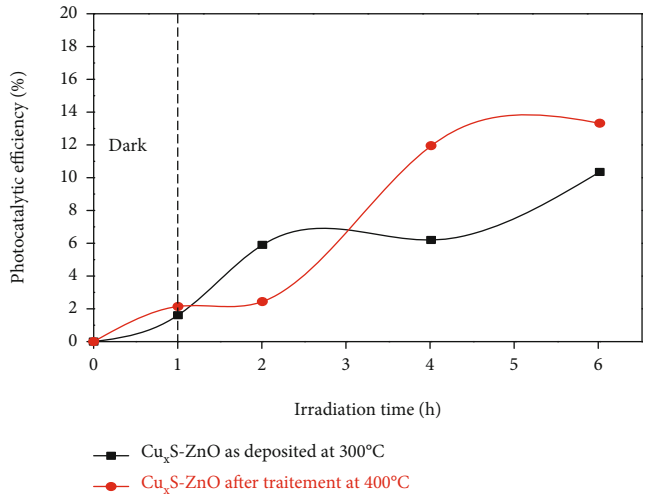

Figure 8: MB photodegradation efficiency using (a) Cu_xS-ZnO as deposited at 300°C and (b) Cu_xS-ZnO annealed at 400°C.

values (VB and CB bands) as illustrated in Figure 7; therefore, in the Cu_xS-ZnO photocatalysts, the holes and electrons were allowed to flow from a semiconductor to another, reducing the electron-hole recombination. A single phase of Cu_xS is difficult to obtain, and the main by-product which is copper oxide can act as a cocatalyst and could therefore lower the activation energy of the set to easily initiate photocatalytic activity. The mechanism of transport and separation of photogenerated electron/hole pair species, related to the different energy bands within the different structures of the constituents of the overall composite material, is illustrated in more detail in Figure 7.

4. Conclusions

A relatively simple, inexpensive, and upscalable method, spray pyrolysis, was used for the deposition of the double

layered composite thin films with the structure glass/-Cu_xS/ZnO, and the formation of these thin films was confirmed by the XRD and EDX analyses. The AFM results prove that the surface roughness increases during annealing as also the crystallinity degree does. The activation energy of the Cu_xS-ZnO composites deposited at 300°C and after annealing at 400°C was estimated based on the Tauc plots as being 2.80 eV and 2.08 eV, respectively, proving the VIS activation of these composites. The photocatalysis results demonstrate that the Cu_xS-ZnO composites after annealing at 400°C have a better photocatalytic response as compared to Cu_xS-ZnO composites deposited at 300°C in the photocatalytic degradation of methylene blue, following a higher crystallinity degree and surface roughness. This deposition method can be further extended to other similarly coupled metal sulfide and metal oxide composite thin films targeting an enhanced photocatalytic VIS-activity.

Data Availability

The data used to support the findings of this study are included within the article. Any other data are available from the corresponding author upon request.

Conflicts of Interest

The authors declare that there is not any conflict of interest.

Funding

The authors acknowledge the award by Agence Universitaire de la Francophonie (AUF) of a mobility/research bursary to APY. The authors also acknowledge the financial support of the Transilvania University of Brasov, R&D Center, Renewable Energy Systems and Recycling.

Supplementary Materials

Table S1: EDX results of the Cu_xS-ZnO composite as deposited at 300°C. Table S2: EDX results of the Cu_xS-ZnO composite after annealing at 400°C. Figure S3: elemental mapping of Cu_xS-ZnO as deposited at 300°C. Figure S4: elemental mapping of Cu_xS-ZnO after annealing at 400°C. Figure S5: absorption spectra variation with time of methylene blue solution under light irradiation using Cu_xS-ZnO as deposited at 300°C. Figure S6: absorption spectra variation with time of Methylene Blue solution under light irradiation using Cu_xS-ZnO annealed at 400°C. *(Supplementary Materials)*

References

[1] B. Lellis, C. Z. Fávaro-Polonio, J. A. Pamphile, and J. C. Polonio, "Effects of textile dyes on health and the environment and bioremediation potential of living organisms," *Biotechnology Research and Innovation*, vol. 3, no. 2, pp. 275–290, 2019.

[2] M. M. Hassan and C. M. A. Carr, "A critical review on recent advancements of the removal of reactive dyes from dyehouse effluent by ion-exchange adsorbents," *Chemosphere*, vol. 209, pp. 201–219, 2018.

[3] D. Fabbri, M. J. López-Muñoz, A. Daniele, C. Medana, and P. Calza, "Photocatalytic abatement of emerging pollutants in pure water and wastewater effluent by TiO_2 and Ce-ZnO: degradation kinetics and assessment of transformation products," *Photochemical & Photobiological Sciences*, vol. 18, no. 4, pp. 845–852, 2019.

[4] E. Regulska, D. Rivera-Nazario, J. Karpinska, M. Plonska-Brzezinska, and L. Echegoyen, "Zinc porphyrin-functionalized fullerenes for the sensitization of titania as a visible-light active photocatalyst: river waters and wastewaters remediation," *Molecules*, vol. 24, no. 6, p. 1118, 2019.

[5] Y. Chen, G. Huang, W. Huang, B. S. Zou, and A. Pan, "Enhanced visible-light photoactivity of La-doped ZnS thin films," *Applied Physics A: Materials Science and Processing*, vol. 108, no. 4, article 6990, pp. 895–900, 2012.

[6] S. A. Ansari, S. G. Ansari, H. Foaud, and M. H. Cho, "Facile and sustainable synthesis of carbon-doped ZnO nanostructures towards the superior visible light photocatalytic performance," *New Journal of Chemistry*, vol. 41, no. 17, pp. 9314–9320, 2017.

[7] A. Naldoni, F. Riboni, U. Guler, A. Boltasseva, V. M. Shalaev, and A. V. Kildishev, "Solar-powered plasmon-enhanced heterogeneous catalysis," *Journal of Nanophotonics*, vol. 5, no. 1, pp. 112–133, 2016.

[8] R. Sedghi and F. A. Heidari, "A Novel & effective visible light-driven TiO2/magnetic porous graphene oxide nanocomposite for the degradation of dye pollutants," *RSC Advances*, vol. 6, no. 55, pp. 49459–49468, 2016.

[9] W. Vallejo, A. Cantillo, B. Salazar et al., "Comparative study of ZnO thin films doped with transition metals (cu and co) for methylene blue photodegradation under visible irradiation," *Catalysts*, vol. 10, no. 5, pp. 528–613, 2020.

[10] M. Basu, N. Garg, and A. K. Ganguli, "A type-II semiconductor (ZnO/CuS heterostructure) for visible light photocatalysis," *Journal of Materials Chemistry A*, vol. 2, no. 20, pp. 7517–7525, 2014.

[11] G. Hitkari, S. Singh, and G. Pandey, "Structural, optical and photocatalytic study of ZnO and ZnO-ZnS synthesized by chemical method," *Nano-Structures & Nano-Objects*, vol. 12, pp. 1–9, 2017.

[12] J. Theerthagiri, R. A. Senthil, A. Malathi, A. Selvi, J. Madhavan, and M. Ashokkumar, "Synthesis and characterization of CuS-WO_3 composite photocatayst for enhanced visible light photocatalytic activity," *RSC Advances*, vol. 5, pp. 52718–52725, 2015.

[13] L. Andronic, L. Isac, and A. Duta, "Photochemical synthesis of copper sulphide/titanium oxide photocatalyst," *Journal of Photochemistry and Photobiology A: Chemistry*, vol. 221, no. 1, pp. 30–37, 2011.

[14] S. Velanganni, S. Pravinraj, P. Immanuel, and R. Thiruneelakandan, "Nanostructure CdS/ZnO heterojunction configuration for photocatalytic degradation of Methylene Blue," *Physical Review B: Condensed Matter*, vol. 534, pp. 56–62, 2018.

[15] G. Mano, S. Harinee, S. Sridhar, M. Ashok, and A. Viswanathan, "Microwave assisted synthesis of ZnO-PbS heterojuction for degradation of organic pollutants under visible light," *Scientific Reports*, vol. 10, no. 1, article 59066, pp. 2224–2314, 2020.

[16] L. Isac, L. Andronic, A. Enesca, and A. Duta, "Copper sulfide films obtained by spray pyrolysis for dyes photodegradation

under visible light irradiation," *Journal of Photochemistry and Photobiology A: Chemistry*, vol. 252, pp. 53–59, 2013.

[17] S. Li, K. Yu, Y. Wang et al., "Cu_2S@ZnO hetero-nanostructures: facile synthesis, morphology-evolution and enhanced photocatalysis and field emission properties," *CrystEngComm*, vol. 15, no. 9, pp. 1753–1761, 2013.

[18] L. Zhu, M. Zheng, J. Lu, M. Xu, and H. J. Seo, "Synthesis of CuS/ZnO Nanocomposite and Its Visible-Light Photocatalytic Activity," *Journal of Nanomaterials*, vol. 2014, Article ID 126475, 7 pages, 2014.

[19] D. Hong, W. Zang, X. Guo et al., "High Piezo-photocatalytic efficiency of CuS/ZnO nanowires using both solar and mechanical energy for degrading organic dye," *ACS Applied Materials & Interfaces*, vol. 8, no. 33, pp. 21302–21314, 2016.

[20] S. S. T. Selvi, H. G. Priya, A. A. Shaly, L. A. Joseph, and J. M. Linet, "Synthesis, characterization, photocatalytic effect of thiourea and thioglycolic acid on ZnO/CuS nanocomposites for degradation of Mordant Black 11 dye," *Applied Physics A*, vol. 126, no. 5, article 3499, pp. 1–14, 2020.

[21] Y. Zhang, B. Huang, P. Li, X. Wang, and Y. Zhang, "Tribological performance of CuS-ZnO nanocomposite film: The effect of CuS doping," *Tribology International*, vol. 58, pp. 7–11, 2013.

[22] W. Y. Kim, S. W. Kim, D. H. Yoo, E. J. Kim, and S. H. Hahn, "Annealing effect of ZnO seed layer on enhancing photocatalytic activity of ZnO/TiO_2 nanostructure," *International Journal of Photoenergy*, vol. 2013, Article ID 130541, 7 pages, 2013.

[23] M. Covei, D. Perniu, C. Bogatu, and A. Duta, "CZTS-TiO_2 thin film heterostructures for advanced photocatalytic wastewater treatment," *Catalysis Today*, vol. 321-322, pp. 172–177, 2019.

[24] M. Andrew, "An overview of the methylene blue ISO test for assessing the activities of photocatalytic films," *Applied Catalysis B: Environmental*, vol. 128, pp. 144–149, 2012.

[25] P. R. Nikam, P. K. Baviskar, J. V. Sali, K. V. Gurav, J. H. Kim, and B. R. Sankapal, "SILAR coated Bi_2S_3 nanoparticles on vertically aligned ZnO nanorods: synthesis and characterizations," *Ceramics International*, vol. 41, no. 9, pp. 10394–10399, 2015.

[26] L. Zhang, J. Huang, J. Yang et al., "The effects of thickness on properties of B and Ga co-doped ZnO films grown by magnetron sputtering," *Materials Science in Semiconductor Processing*, vol. 42, pp. 277–282, 2016.

[27] D. K. Kim and C. B. Park, "Deposition of ZnO thin films on Si by RF magnetron sputtering with various substrate temperatures," *Journal of Materials Science: Materials in Electronics*, vol. 25, no. 12, article 2322, pp. 5416–5421, 2014.

[28] M. Jing, F. Li, M. Chen et al., "Facile synthetic strategy to uniform Cu_9S_5 embedded into carbon: a novel anode for sodium-ion batteries," *Journal of Alloys and Compounds*, vol. 762, pp. 473–479, 2018.

[29] D. Wu, X. Fan, J. Dai, H. Liu, H. Liu, and F. Zhang, "Preparation and photocatalytic properties of Cu2S/tetrapod-like ZnO whisker nanocomposites," *Chinese Journal of Catalysis*, vol. 33, no. 4-6, pp. 802–807, 2012.

[30] A. Enesca, L. Isac, and A. Duta, "Hybrid structure comprised of SnO_2, ZnO and Cu_2S thin film semiconductors with controlled optoelectric and photocatalytic properties," *Thin Solid Films*, vol. 542, pp. 31–37, 2013.

[31] O. A. Carrasco-Jaim, O. Ceballos-Sanchez, L. M. Torres-Martínez, E. Moctezuma, and C. Gómez-Solís, "Synthesis and characterization of PbS/ZnO thin film for photocatalytic hydrogen production," *Journal of Photochemistry and Photobiology A: Chemistry*, vol. 347, pp. 98–104, 2017.

[32] A. Enesca, A. Andronic, and A. Duta, "Optimization of opto-electrical and photocatalytic properties of SnO_2 thin films using Zn^{2+} and W^{6+} dopant ions," *Catalysis Letters*, vol. 142, no. 2, pp. 224–230, 2012.

[33] C. M. Malengreaux, M. L. Léonard, S. L. Pirard et al., "How to modify the photocatalytic activity of TiO_2 thin films through their roughness by using additives. A relation between kinetics, morphology and synthesis," *Chemical Engineering Journal*, vol. 243, pp. 537–548, 2014.

[34] C. M. Firdaus, M. B. Rizam, M. Rusop, and R. S. Hidayah, "Characterization of ZnO and ZnO: TiO_2 thin films prepared by sol-gel spray- spin coating technique," *Procedia Engineering*, vol. 41, pp. 1367–1373, 2012.

[35] A. López-Suárez, D. Acosta, C. Magaña, and F. Hernández, "Optical, structural and electrical properties of ZnO thin films doped with Mn," *Journal of Materials Science: Materials in Electronics*, vol. 31, no. 10, article 2830, pp. 7389–7397, 2020.

[36] F. Achouri, S. Corbel, L. Balan et al., "Porous Mn-doped ZnO nanoparticles for enhanced solar and visible light photocatalysis," *Materials & Design*, vol. 101, pp. 309–316, 2016.

[37] L. Isac, I. Popovici, A. Enesca, and A. Duta, "Copper sulfide (Cu_xS) thin films as possible p-type absorbers in 3D solar cells," *Energy Procedia*, vol. 2, no. 1, pp. 71–78, 2010.

[38] M. Adelifard, H. Eshghi, and M. M. Bagheri Mohagheghi, "Synthesis and characterization of nanostructural CuS-ZnS binary compound thin films prepared by spray pyrolysis," *Optics Communication*, vol. 285, no. 21-22, pp. 4400–4404, 2012.

[39] S. Islam, M. A. Hussain, and M. J. Rashid, "Deposition and optical characterization of ZnO thin films on glass substrate," *Journal de Physique*, vol. 1086, article 012009, 2018.

[40] A. Duta, A. Enesca, C. Bogatu, and E. Gyorgy, "Solar-active photocatalytic tandems. A compromise in the photocatalytic processes design," *Materials Science in Semiconductor Processing*, vol. 42, pp. 94–97, 2016.